Supplementary Information for

Heterogeneous Interface on NiS@Ni_3S_2/$NiMoO_4$ Heterostructures for Efficient Urea Electrolysis

Linna Sha,[a,+] Tianfu Liu,[b,+] Ke Ye,[a,*] Kai Zhu,[a] Jun Yan,[a] Jinling Yin,[a] Guiling Wang,[a] Dianxue Cao[a,*]

[a] Key Laboratory of Superlight Materials and Surface Technology of Ministry of Education, College of Materials Science and Chemical Engineering, Harbin Engineering University, Harbin, 150001, China.

[b] State Key Laboratory of Catalysis, Dalian National Laboratory for Clean Energy, Dalian Institute of Chemical Physics, Chinese Academy of Sciences, Dalian 116023, China.

[+] These authors contributed equally to this work.
[*]Corresponding authors.
E-mail addresses: yeke@hrbeu.edu.cn (K. Ye); caodianxue@hrbeu.edu.cn (D. Cao)

Experimental

Synthesis of NiS@Ni_3S_2 nanorod arrays framework. In a typical synthesis, 5 mmol sulfur powder was dispersed in 16 mL $C_2H_8N_2$ with homogenously stirred for 10 min, and then 16 mL ethanol was added to the above solution and rapid stirring for 10 min. Next, the mixture was transferred into a 50 mL Teflon-lined stainless autoclave containing the precleaned Ni foam (2.0 cm×3.0 cm). After hydrothermal treating at 160 ^oC for 24 h, the products were collected and then cleaned by deionized water and ethanol several times before they were dried under vacuum at 60 ^oC for overnight.

Synthesis of NiS@Ni_3S_2/$NiMoO_4$ composite. First, 0.01 g sodium molybdate and 0.014 g nickel nitrate were dispersed into 50 mL of 50 wt% aqueous ethanol solution. Subsequently, the as-obtained NiS@Ni_3S_2 was immersed in the solution and reacted in a 50 mL Teflon-lined autoclave at 130 ^oC for 12 h. After cooled down to room temperature, the Ni foam with prepared precursors were transferred to muffle furnace and annealed at 400 ^oC for 2 h in air atmosphere to obtain the NiS@Ni_3S_2/$NiMoO_4$ composite.

For comparison, $NiMoO_4$ grown on Ni foam were obtained in the similarly procedure by replacing NiS@Ni_3S_2 with pure Ni foam.

Material Characterizations

The crystal configuration of the samples was identified by X-ray diffractometer (Rigaku TTR III) with a Cu_{Ka} radiation (λ=1.5418 nm). The scanning electron microscope (SEM) with energy dispersive X-ray spectroscopy (EDX) were taken with JEOL JSM-6480 system. Transmission electron microscopy (TEM) and high resolution

TEM (HRTEM) images were collected on a JEOL-2100F TEM at an acceleration voltage of 200 kV. X-ray photoelectron spectroscopy (XPS) measurements were carried out using the surface analysis system (Thermofisher Escalab Xi^+) with a monochromatic $Al_{K\alpha}$ X-ray source (hν=1486.6 eV).

Electrochemical Measurements

Electrochemical measurements were carried out in an electrochemical workstation (Autolab PGSTAT 302) with a typical three-electrode system, in which the resultant catalyst with a dimensions of 1.0 cm×1.0 cm was directly served as the working electrode, The carbon rod and Ag/AgCl electrode were used as the working electrode, counter electrode and reference electrode, respectively. After weighed the active materials loads per unit area, the mass loading of NiS@Ni_3S_2, $NiMoO_4$/NF and NiS@Ni_3S_2/$NiMoO_4$ catalysts are 0.0312 g, 0.0326 g and 0.0326 g, respectively. All linear sweep voltammetry (LSV) were carried out with a scan rate of 2 mV s^{-1}. All measured potentials were calibrated to reversible hydrogen electrode (RHE) according to the following equation: $E_{RHE}=E_{Ag/AgCl}$ + 0.197 + 0.059×pH. The measured UOR polarization curves were capacity corrected by taking an average of forward and backward scans. The electrochemically active surface areas (ECSA) were estimated by a series of cyclic voltammetry measurements performed with various scan rates (20~100 mV s^{-1}) in a non-Faradaic region. By plotting the difference of current density (ΔJ) between the anodic and cathodic sweeps (J_{anodic}–$J_{cathodic}$) under intermediate potential against the scan rate, a linear trend was observed. The slope of the fitting line is equal to twice the geometric double layer capacitance (C_{dl}), which is proportional to

the ECSA of the catalyst. Therefore, we can compare the electrochemical surface areas of different samples based on their C_{dl} values. Electrochemical impedance spectra (EIS) were collected at a frequency between 100 kHz and 0.01 kHz. In water splitting tests, all results were revised by ohmic potentials drop (*iR*) correction. The electrolyte for HER, OER and water electrolysis measurements was 1 M KOH, whereas the UOR and urea electrolysis performance were evaluated in 1 M KOH with 0.5 M urea. The stability measurements were recorded by chronopotentiometry measurements.

Calculations

The simulated model in this work consists of a slab of NiS ($Ni_{36}S_{36}$), and $NiMoO_4$ ($Ni_8Mo_8O_{32}$). The calculations presented here were performed using the periodic, spin-polarized DFT as implemented in the Vienna ab initio simulation package (VASP).[1] The electron-ion interactions were described by the projector augmented wave (PAW) method proposed by Blochl[2] and implemented by Kresse.[3] The RPBE functional was used as an exchange-correlation functional approximation[4] and a plane wave basis set with an energy cutoff of 400 eV was used. Only gamma point was used for the Brillouin zone sampling.

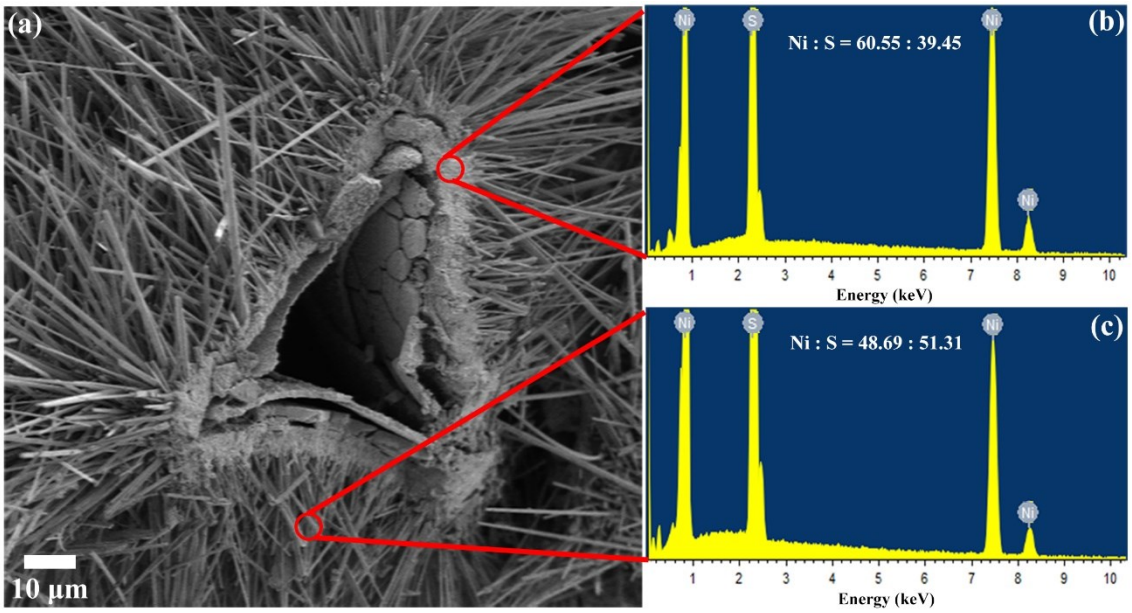

Figure S1. (a) Cross-sectional SEM image and the EDX spectra of the (b) internal framework and (c) external nanorods of the NiS@Ni_3S_2 sample.

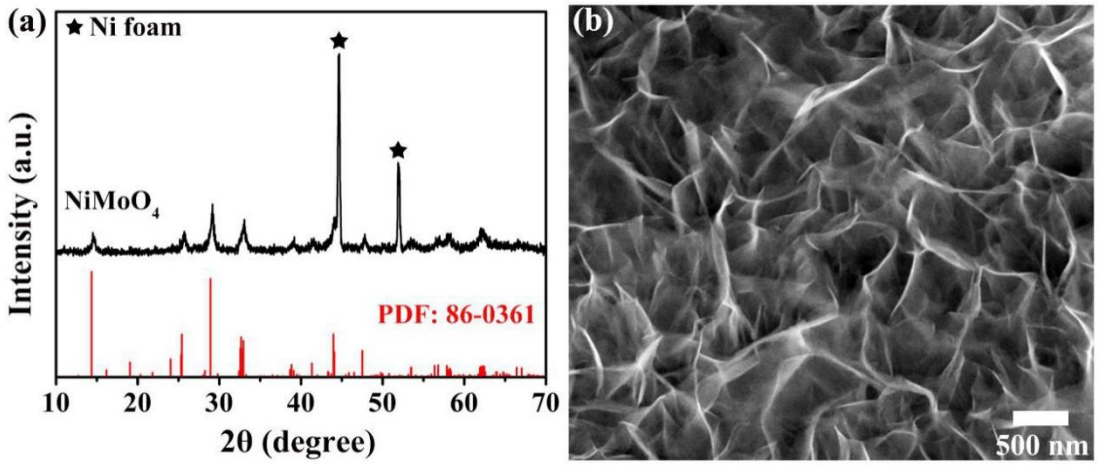

Figure S2. (a) XRD pattern and (b) SEM image of $NiMoO_4$ nanosheets grown on the Ni foam.

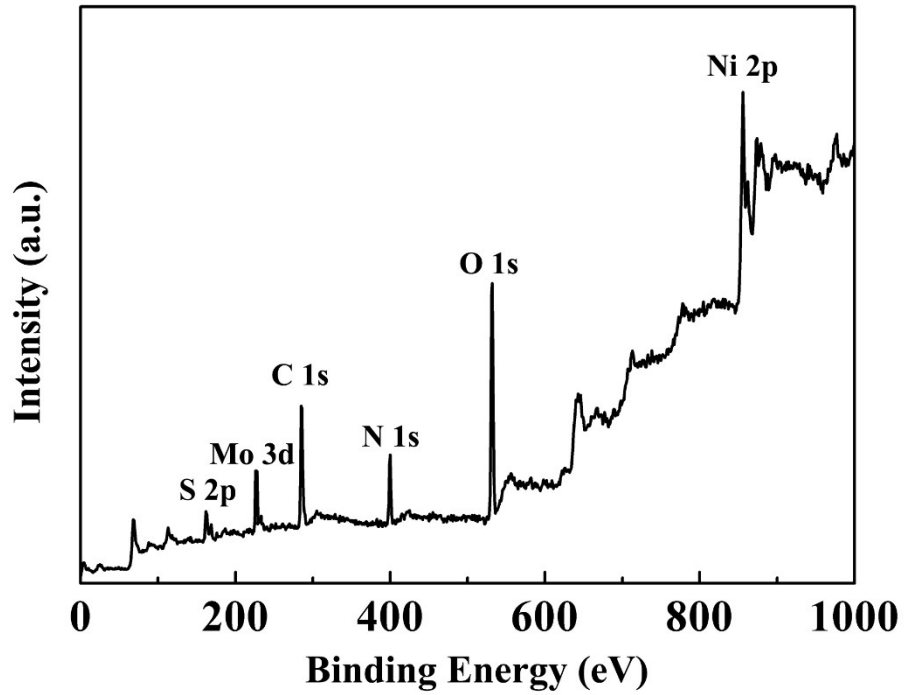

Figure S3. Full XPS survey spectrum of $NiS@Ni_3S_2/NiMoO_4$.

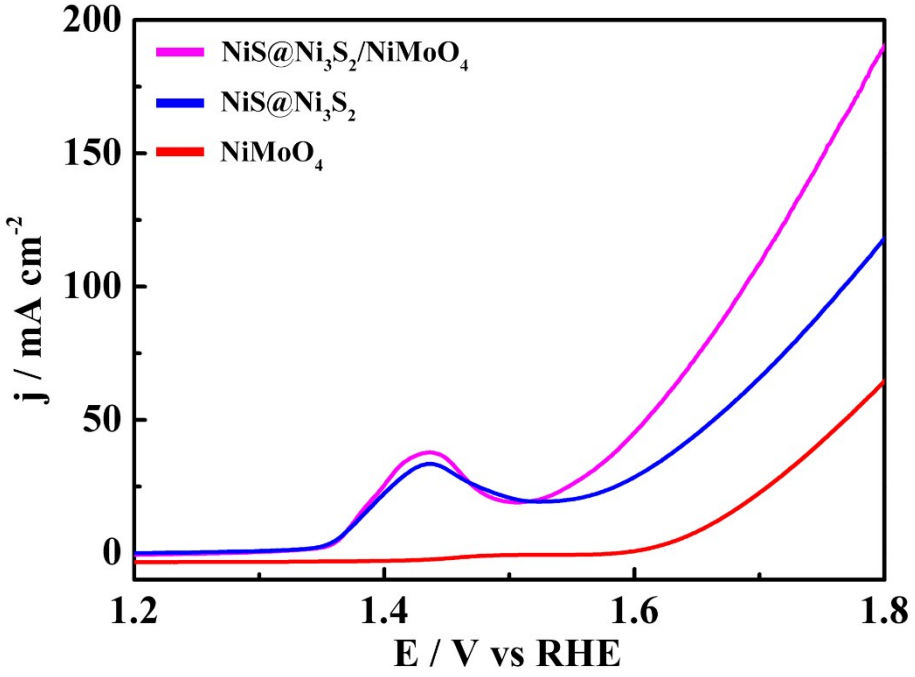

Figure S4. OER polarization curves of $NiMoO_4$, $NiS@Ni_3S_2$ and $NiS@Ni_3S_2/NiMoO_4$ in 1.0 M KOH.

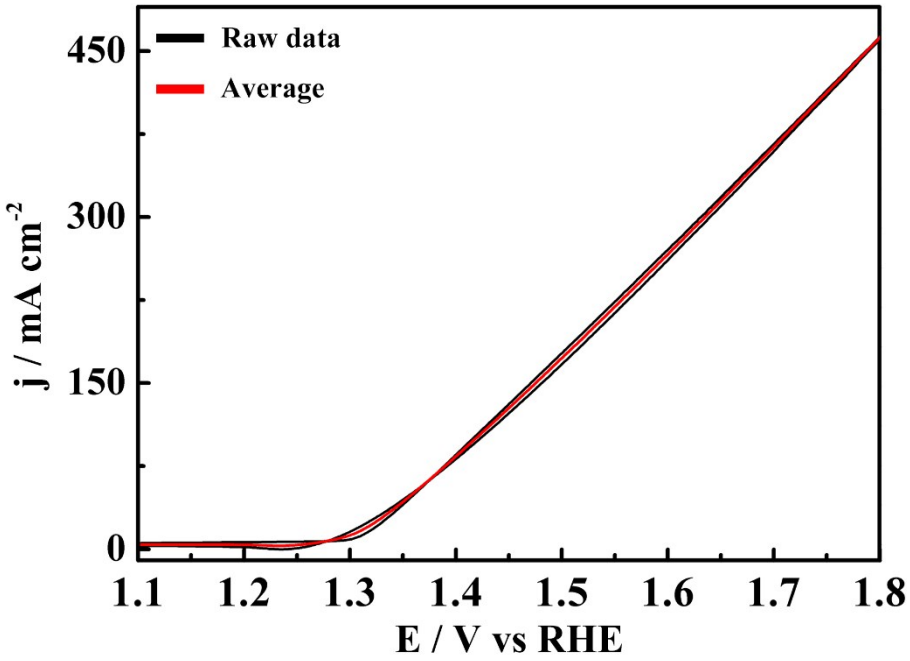

Figure S5. Cyclic voltammetry (CV) curve (black) and corresponding average activity calculated from the CV curve (red) of NiS@Ni_3S_2/$NiMoO_4$ electrode. Scan rate: 2 mV s^{-1}.

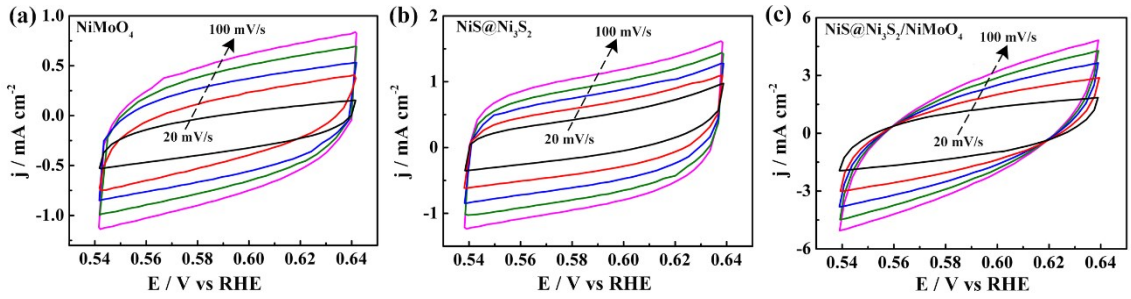

Figure S6. Cyclic voltammetry curves for (a) $NiMoO_4$, (b) NiS@Ni_3S_2 and (c) NiS@Ni_3S_2/$NiMoO_4$ electrodes in the region of 0.54~0.64 V vs. RHE with different scan rates upon UOR catalysis.

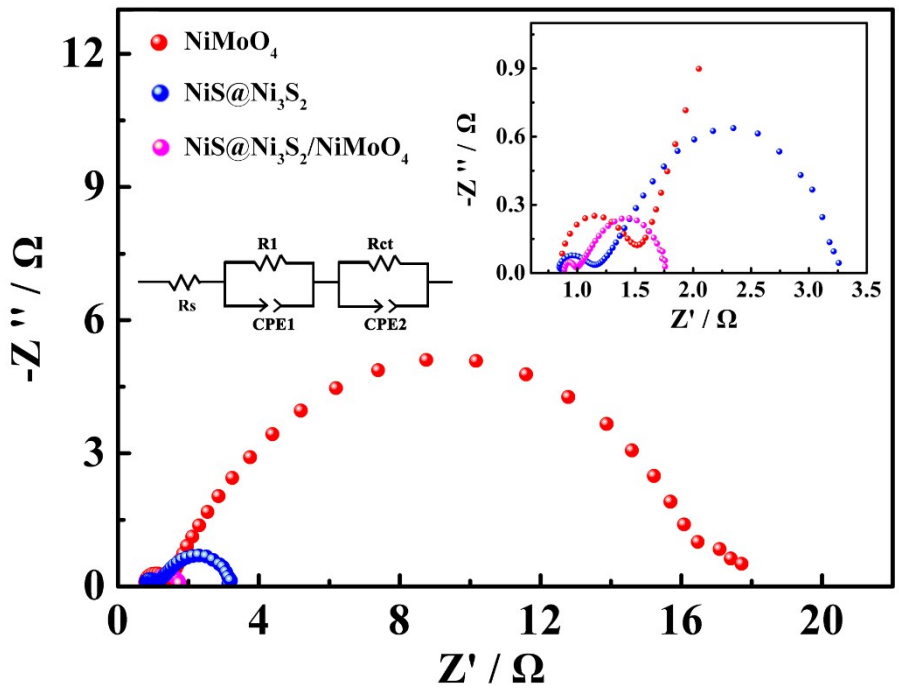

Figure S7. Nyquist plots of $NiMoO_4$, $NiS@Ni_3S_2$ and $NiS@Ni_3S_2/NiMoO_4$ catalysts for UOR process at 1.35 V vs. RHE.

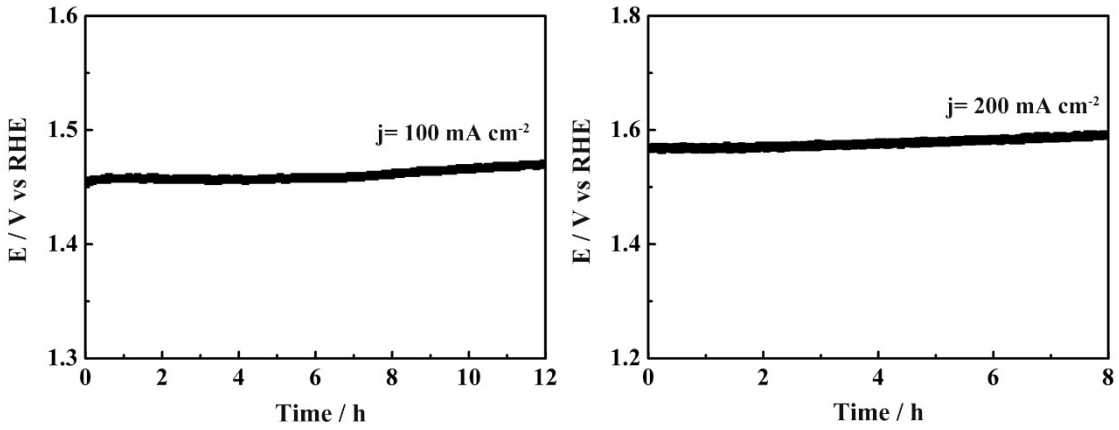

Figure S8. Long-time stability test of $NiS@Ni_3S_2/NiMoO_4$ at (a) 100 and (b) 200 mA cm^{-2} for 12 and 8 h, respectively.

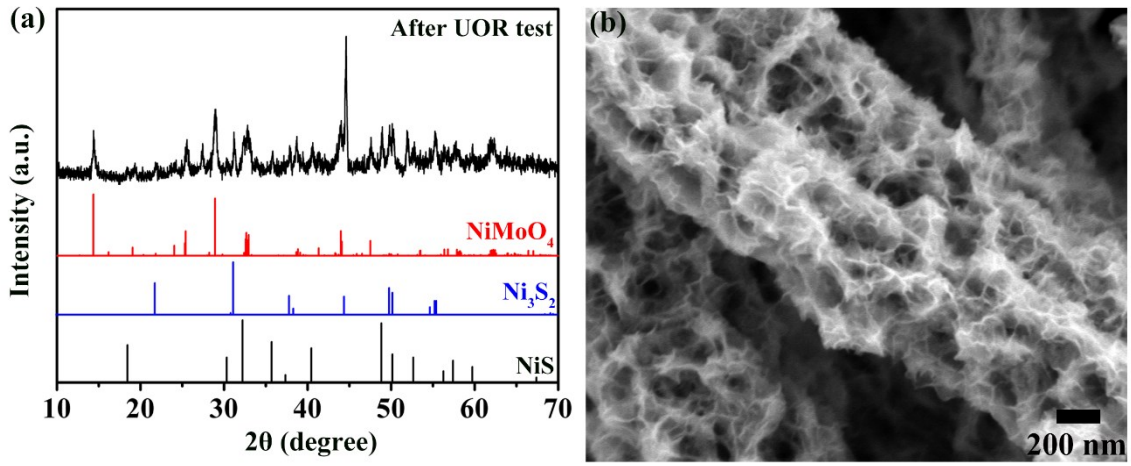

Figure S9. (a) XRD pattern and (b) SEM image of NiS@Ni_3S_2/$NiMoO_4$ after UOR test.

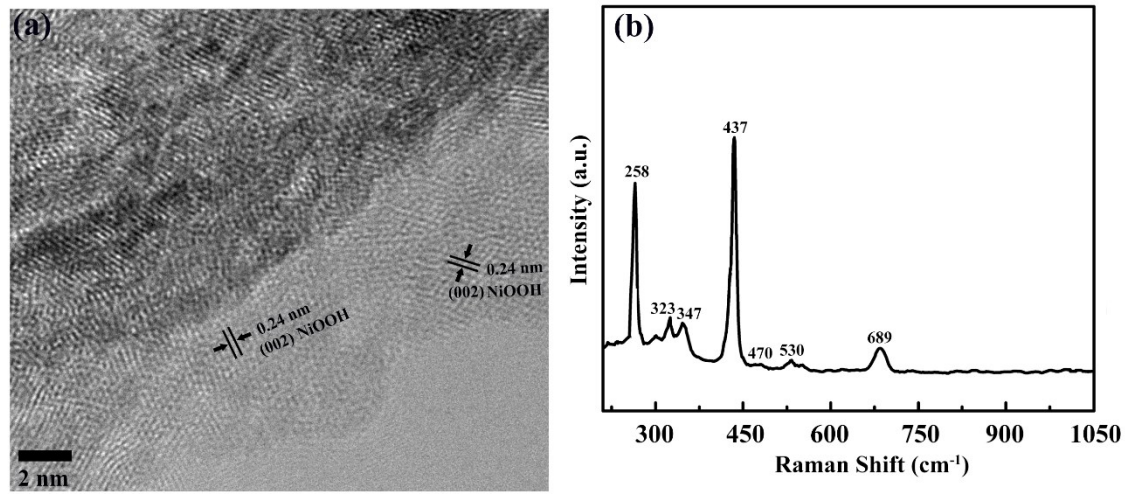

Figure S10. (a) HRTEM image and (b) Raman spectrum of NiS@Ni_3S_2/$NiMoO_4$ after UOR test.

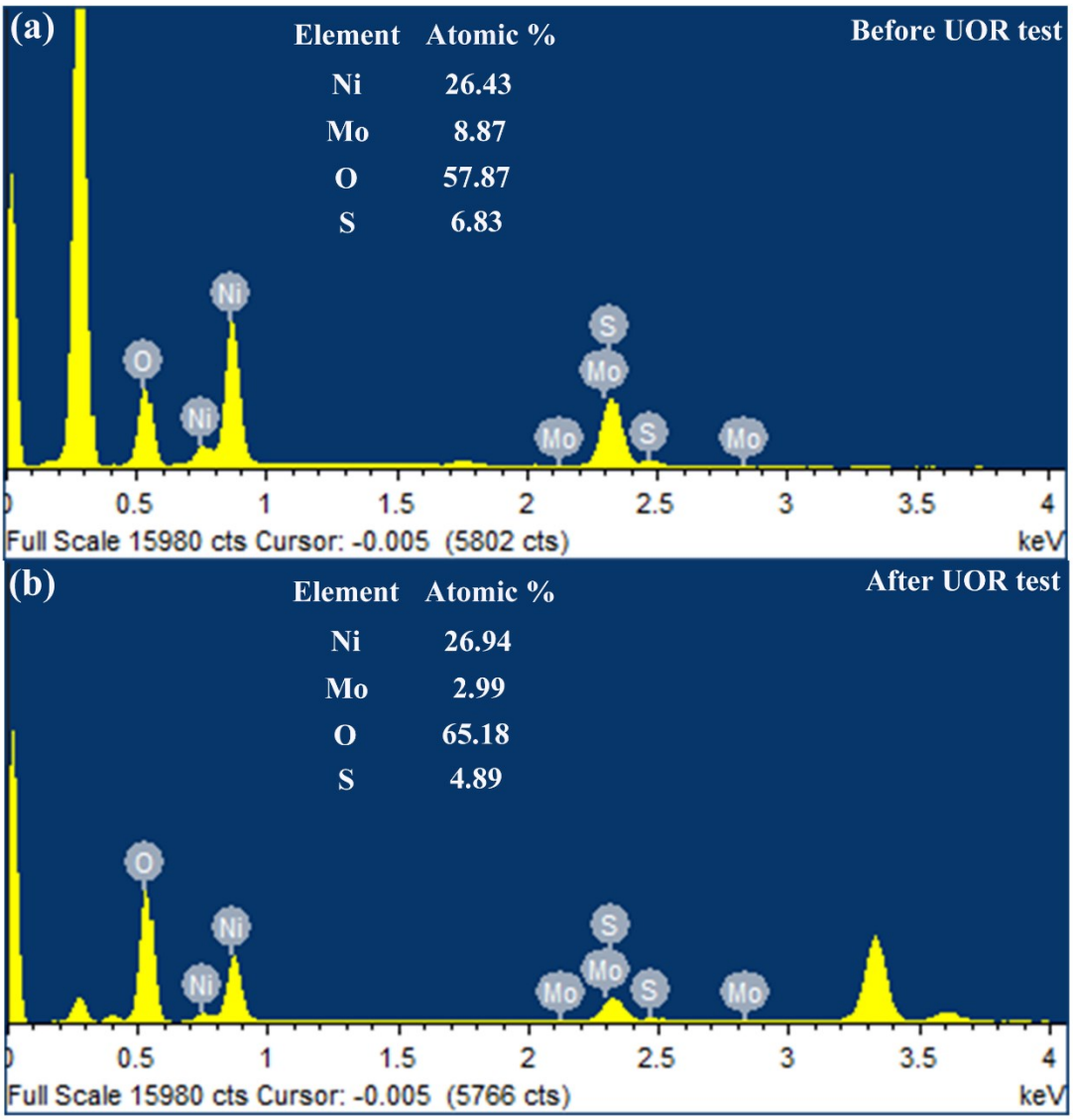

Figure S11. EDX spectra of NiS@Ni_3S_2/$NiMoO_4$ catalyst (a) before and (b) after UOR test.

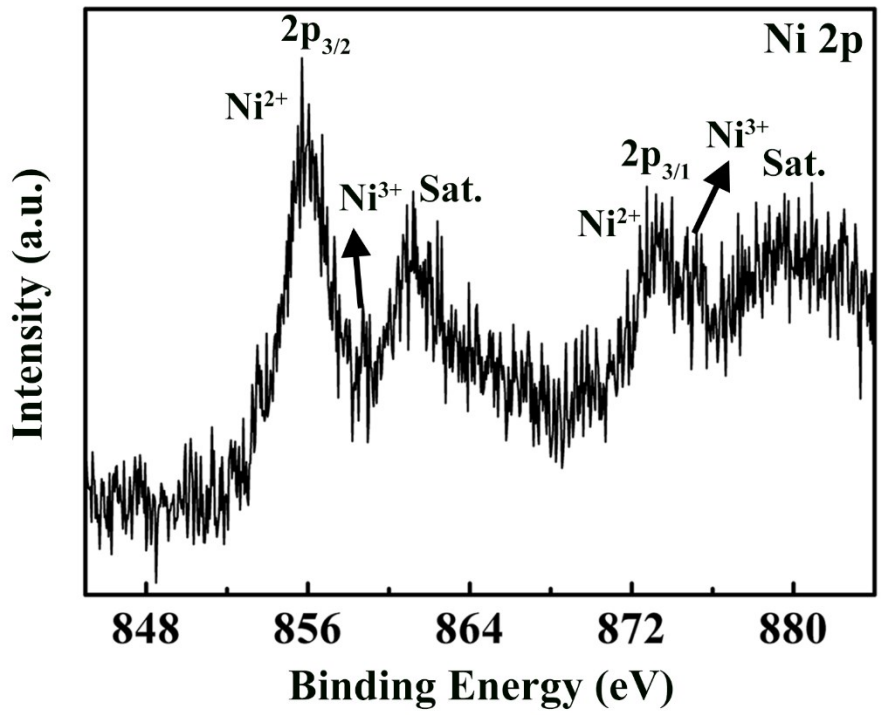

Figure S12. High resolution Ni 2p spectrum of NiS@Ni_3S_2/$NiMoO_4$ after UOR test.

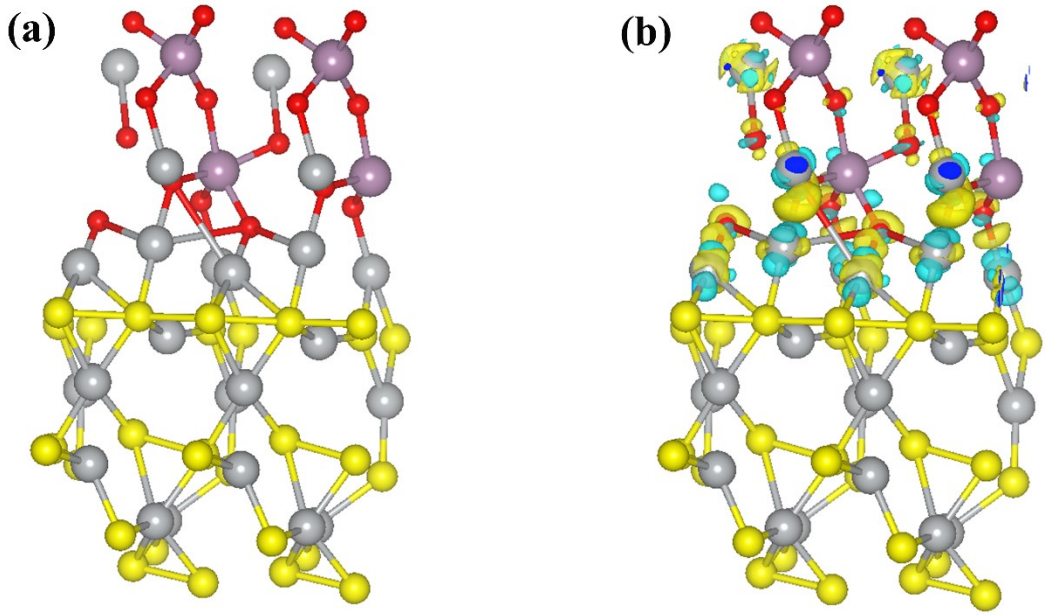

Figure S13. (a) The heterojunction structure of NiS/$NiMoO_4$ with (010) facet. The gray, red, yellow, purple spheres represent nickel, oxygen, sulfur, and molybdenum atoms, respectively. (b) The charge density difference in the heterostructure of NiS and $NiMoO_4$. The yellow and blue isosurfaces represent charge accumulation and charge depletion in space, respectively.

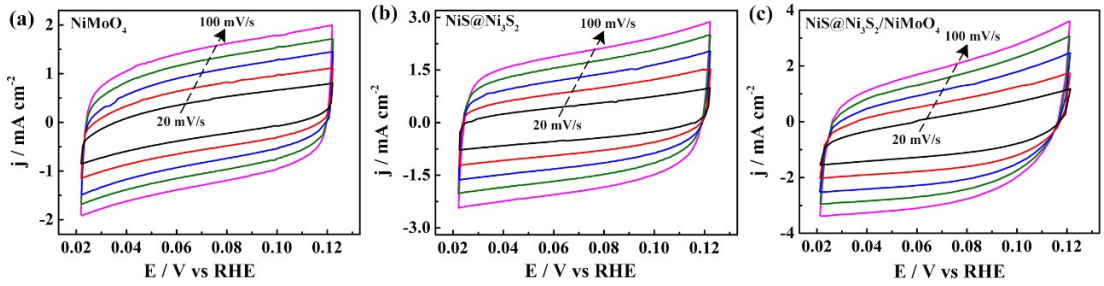

Figure S14. Cyclic voltammetry curves for (a) $NiMoO_4$, (b) $NiS@Ni_3S_2$ and (c) $NiS@Ni_3S_2/NiMoO_4$ electrodes in the region of 0.02~0.12 V vs. RHE with different scanning rates upon HER catalysis.

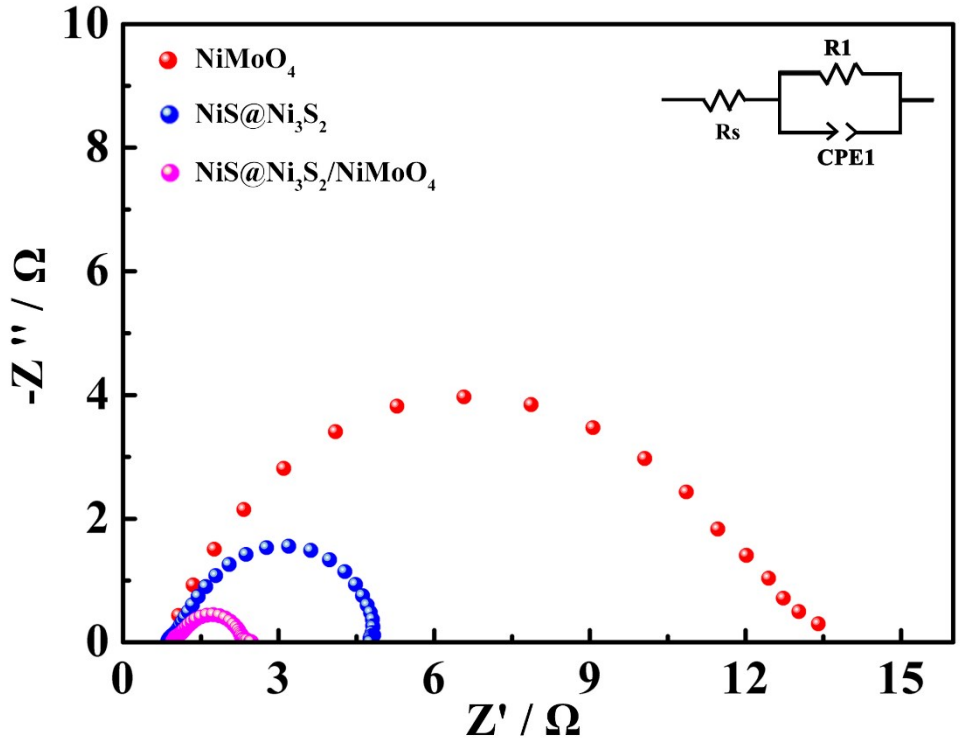

Figure S15. Nyquist plots of $NiMoO_4$, $NiS@Ni_3S_2$ and $NiS@Ni_3S_2/NiMoO_4$ catalysts for HER process at an overpotential of –200 mV.

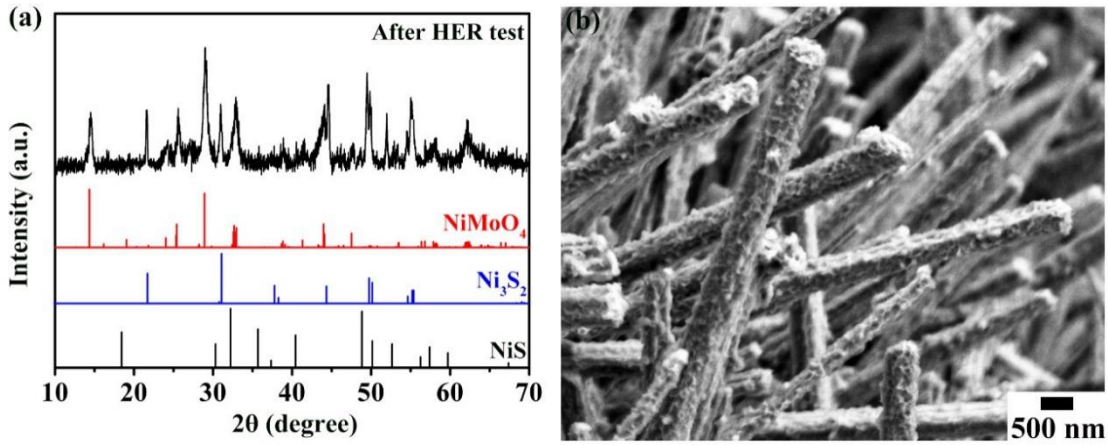

Figure S16. (a) XRD pattern and (b) SEM image of NiS@Ni_3S_2/$NiMoO_4$ after HER test.

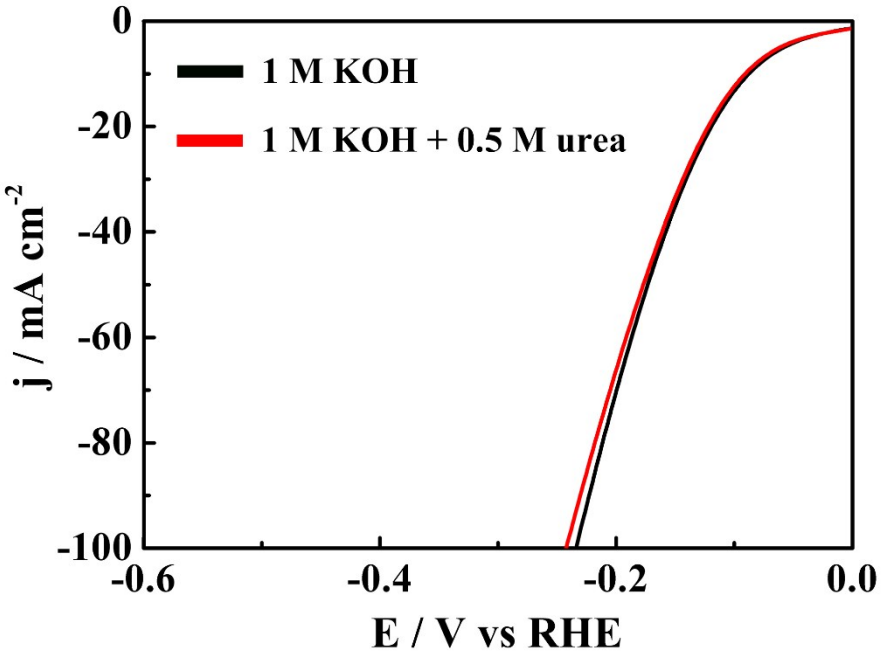

Figure S17. HER polarization plots of NiS@Ni_3S_2/$NiMoO_4$ in 1 M KOH with and without 0.5 M urea.

Table S1. Comparison of the UOR performance of $NiS@Ni_3S_2/NiMoO_4$ with other reported non-precious electrocatalysts in 1 M KOH electrolyte.

Catalysts	Urea concentrate (M)	j (mA cm^{-2})	Voltage (V vs RHE)	Tafel slope (mV dec^{-1})	References
$NF/NiMoO_4$	0.5	10	1.37	19	[5]
Ni_3N/NF	0.5	10	1.34	41	[6]
MoS_4-LDH/NF	0.33	10	1.34	29	[7]
$MnO_2/MnCo_2O_4/Ni$	0.5	10	1.33	72	[8]
Ni_2P/NF	0.5	10	1.37	49	[9]
NF/MnO_2	0.5	10	1.33	75	[10]
Ni-Mo alloy	0.1	10	1.36	22	[11]
NiMoS/Ti	0.5	10	1.34	19	[12]
$NiS@Ni_3S_2/NiMoO_4$	0.5	10	1.30	30	This work

Table S2. Comparison of the HER performance of $NiS@Ni_3S_2/NiMoO_4$ with other reported electrocatalysts in 1 M KOH electrolyte.

Catalysts	j ($mA\ cm^{-2}$)	η_j (mV)	Tafel slope ($mV\ dec^{-1}$)	References
$MoSe_2/SnO_2$	10	174	51	[13]
Ni_3S_2/NiS/NOSC	10	180	83	[14]
$Ni_{0.89}Co_{0.11}Se_2$ MNSN/NF	10	85	52	[15]
MoS_2-Ni_3S_2	10	110	83	[16]
S-$MoSe_2$	10	100	60	[17]
$Co_3S_4@MoS_2$	10	136	74	[18]
CF@NPC-MoP	10	53	55.6	[19]
Co_3S_4/EC-MOF	10	84	82	[20]
N-$MoSe_2$/TiC-C	10	106	32	[21]
$NiS@Ni_3S_2/NiMoO_4$	10	80	75	This work

Table S3. Comparison of the urea electrolysis efficiency of $NiS@Ni_3S_2/NiMoO_4$ with other reported bifunctional electrocatalysts.

Catalysts	Electrolyte	Cell voltage (V)	j ($mA\ cm^{-2}$)	References
NiMoS/CC	1.0 M KOH+0.5 M urea	1.59	10	[12]
Ni_3N/CC	1.0 M KOH+0.33 M urea	1.44	10	[22]
$MnO_2/MnCo_2O_4$/NF	1.0 M KOH+0.5 M urea	1.55	10	[8]
CoS_2/Ti	1.0 M KOH+0.3 M urea	1.59	10	[23]
$Fe_{11.1\%}$-Ni_3S_2/NF	1.0 M KOH+0.33 M urea	1.46	10	[24]
Ni-Mo alloy	1.0 M KOH+0.1 M urea	1.43	10	[11]
1% Cu:a$Ni(OH)_2$/NF	1.0 M KOH+0.33 M urea	1.49	10	[25]
NiFeCo LDH/NF	1.0 M KOH+0.33 M urea	1.49	10	[26]
Ni_2P/Fe_2P	1.0 M KOH+0.5 M urea	1.47	10	[27]
$NiS@Ni_3S_2/NiMoO_4$	1.0 M KOH+0.5 M urea	1.40	10	This work

References

[1] G. Kresse and J. Furthmüller, *Phys. Rev. B*, 1996, **54**, 11169-11186.

[2] G. Kresse and J. Furthmüller, *Comp. Mater. Sci*., 1996, **6**, 15-50.

[3] P. E. Blöchl and Matter, *Phys. Rev. B*, 1994, **50**, 17953-17979.

[4] B. Hammer, L. B. Hansen and J. K. Nørskov, *Phys. Rev. B*, 1999, **59**, 7413-7421.

[5] Z. Y. Yu, C. C. Lang, M. R. Gao, Y. Chen, Q. Q. Fu, Y. Duan and S. H. Yu, *Energy Environ. Sci*., 2018, **11**, 1890-1897.

[6] S. Hu, C. Feng, S. Wang, J. Liu, H. Wu, L. Zhang and J. Zhang, *ACS Appl. Mater. Interfaces*, 2019, **11**, 13168-13175.

[7] A. Nadeema, V. Kashyap, R. Gururaj and S. Kurungot, *ACS Appl. Mater. Interfaces*, 2019, **11**, 25917-25927.

[8] C. Xiao, S. Li, X. Zhang and D. R. MacFarlane, *J. Mater. Chem. A*, 2017, **5**, 7825-7832.

[9] D. Liu, T. Liu, L. Zhang, F. Qu, G. Du, A. M. Asiri and X. Sun, *J. Mater. Chem. A*, 2017, **5**, 3208-3213.

[10] S. Chen, J. Duan, A. Vasileff and S. Z. Qiao, *Angew. Chem. Int. Ed*., 2016, **55**, 3804-3808.

[11] J. Y. Zhang, T. He, M. Wang, R. Qi, Y. Yan, Z. Dong, H. Liu, H. Wang and B. Y. Xia, *Nano Energy*, 2019, **60**, 894-902.

[12] X. Wang, J. Wang, X. Sun, S. Wei, L. Cui, W. Yang and J. Liu, *Nano Res*., 2018, **11**, 988-996.

[13] Y. Huang, Y. E. Miao, J. Fu, S. Mo, C. Wei and T. Liu, *J. Mater. Chem. A*, 2015,

3, 16263-16271.

[14]Y. Cao, Y. Meng, S. Huang, S. He, X. Li, S. Tong and M. Wu, *ACS Sustain. Chem. Eng*., 2018, **6**, 15582-15590.

[15] B. Liu, Y. F. Zhao, H. Q. Peng, Z. Y. Zhang, C. K. Sit, M. F. Yuen, T. R. Zhang, C. S. Lee and W. J. Zhang, *Adv. Mater*., 2017, **29**, 1606521.

[16] J. Zhang, T. Wang, D. Pohl, B. Rellinghaus and R. J. Dong, *Angew. Chem. Int. Ed*., 2016, **55**, 6702-6707.

[17] C. Xu, S. J. Peng, C. L. Tan, H. X. Ang, H. T. Tan, H. Zhang and Q. Y. Yan, *J. Mater. Chem. A*, 2014, **2**, 5597-5601.

[18] Y. Guo, J. Tang, Z. Wang, Y. M. Kang, Y. Bando and Y. Yamauchi, *Nano Energy*, 2018, **47**, 494-502.

[19] J. Xiao, Z. Zhang, Y. Zhang, Q. Lv, F. Jing, K. Chi and S. Wang, *Nano Energy*, 2018, **51**, 223-230.

[20] T. Liu, P. Li, N. Yao, T. Kong, G. Cheng, S. Chen and W. J. Luo, *Adv. Mater*., 2019, **31**, 1806672.

[21] S. Deng, Y. Fan, Q. H. Zhang and Z. Yu, *Adv. Mater*., 2018, **30**, 1802223.

[22] Q. Liu, L. Xie, F. Qu, Z. Liu, G. Du, A. M. Asiri and X. Sun, *Inorg. Chem. Front*., 2017, **4**, 1120-1124.

[23] S. Wei, X. Wang, J. Wang, X. Sun, L. Cui, W. Yang, Y. Zheng and J. Liu, *Electrochim. Acta*, 2017, **246**, 776-782.

[24] W. Zhu, Z. Yue, W. Zhang, N. Hu, Z. Luo, M. Ren, Z. Xu, Z. Wei, Y. Suo and J. Wang, *J. Mater. Chem. A*, 2018, **6**, 4346-4353.

[25] J. Xie, L. Gao, S. Cao, W. Liu, F. Lei, P. Hao, X. Xia and B. Tang, *J. Mater. Chem. A*, 2019, **7**, 13577-13584.

[26] P. Babar, A. Lokhande, V. Karade, B. Pawar, M. G. Gang, S. Pawar and J. H. Kim, *ACS Sustain. Chem. Eng*., 2019, **7**, 10035-10043.

[27] L. Yan, Y. Sun, E. Hu, J. Ning, Y. Zhong, Z. Zhang and Y. Hu, *J. Colloid Interf. Sci*., 2019, **541**, 279-286.